PHYSICAL REVIEW B **92**, 045210 (2015)

Measuring anisotropic resistivity of single crystals using the van der Pauw technique

Kasper A. Borup,[1,*] Karl F. F. Fischer,[1] David R. Brown,[2] G. Jeffrey Snyder,[2,3] and Bo B. Iversen[1]

[1] *Center for Materials Crystallography, Department of Chemistry and iNANO, Aarhus University, DK-8000 Aarhus, Denmark*

[2] *Materials Science, California Institute of Technology, Pasadena, California 91125, USA*

[3] *ITMO University, Saint Petersburg, Russia*

(Received 11 February 2015; revised manuscript received 16 June 2015; published 24 July 2015)

Anisotropy in properties of materials is important in materials science and solid-state physics. Measurement of the full resistivity tensor of crystals using the standard four-point method with bar shaped samples requires many measurements and may be inaccurate due to misalignment of the bars along crystallographic directions. Here an approach to extracting the resistivity tensor using van der Pauw measurements is presented. This reduces the number of required measurements. The theory of the van der Pauw method is extended to extract the tensor from parallelogram shaped samples with known geometry. Methods to extract the tensor for both known and unknown principal axis orientation are presented for broad applicability to single crystals. Numerical simulations of errors are presented to quantify error sources. Several benchmark experiments are performed on isotropic graphite samples to verify the internal consistency of the developed theory, test experimental precision, and characterize error sources. The presented methods are applied to a $RuSb_2$ single crystal at room temperature and the results are discussed based on the error source analysis. Temperature resolved resistivities along the *a* and *b* directions are finally reported and briefly discussed.

DOI: 10.1103/PhysRevB.92.045210 PACS number(s): 72.20.−i, 81.70.−q, 84.60.Rb

I. INTRODUCTION

The directional dependence of transport and thermodynamic properties is of interest to many fields of materials science and solid-state physics [1]. Examples are magnetism, the thermoelectric effects, thermal and electrical transport, and mechanical properties [2]. The electrical conductivity or resistivity is of high importance to any field dealing with electronic materials, including photovoltaics, topological insulators, and thermoelectrics. The precision of resistivity measurements is high, i.e., low variation with repeated measurements. The variation can often be less than 1% [3]. This makes resistivity a good property for initially testing materials for anisotropy, even when this is not the property of interest.

In thermoelectrics the resistivity is of high importance as it accounts for efficiency reduction due to parasitic power loss from Joule heating. Many thermoelectric materials of interest possess complex structures which are often anisotropic [4]. $RuSb_2$ is a narrow gap semiconductor of interest as an isoelectronic and isostructural reference to $FeSb_2$. $FeSb_2$, in turn, has a record high thermopower at cryogenic temperatures and a highly correlated electron structure [5,6]. Both materials have orthorhombic unit cells and are highly anisotropic at low temperatures. Another important example is Bi_2Te_3 based materials, which are used in most commercial Peltier modules and are being investigated as topological insulators [7–9]. These materials are anisotropic and directionally resolved measurements are important for accurate characterization [10–12]. A recent example is the novel high efficiency thermoelectric material SnSe [13,14]. Accurate measurement of thermoelectric transport properties is important to evaluate the performance of materials [3,15,16]. Easy measurement of anisotropic resistivity can increase the reliability of studies by detecting anisotropic properties.

The most widely used method for measuring resistivity is the four-point bar method. In this method, the resistance R of a bar shaped sample with cross sectional area A and voltage lead separation l is measured. From this the resistivity ρ is calculated as $\rho = RA/l$. If the bar is cut along the $\hat{\boldsymbol{x}}$ unit vector (usually from a single crystal) the measured resistivity relates to the total resistivity tensor as $\rho_{\hat{\boldsymbol{x}}} = \hat{\boldsymbol{x}}^{\mathrm{T}}\rho\hat{\boldsymbol{x}}$. To extract the full tensor at least as many uniquely oriented bars as unique tensor elements are needed. This number is defined by the crystal point group through Neumann's principle [2,17,18]. The four-point bar method is known to potentially be imprecise due to the difficulty of accurately measuring the geometric A/l factor [15]. In anisotropic materials an additional source of error arises from aligning the bar along the direction of interest.

Alternatively, methods using planar samples may be adapted to extract the tensor elements. One such method is the van der Pauw (vdP) method [19,20], which is extensively used in thermoelectrics [21]. This method accepts planar samples of arbitrary shape and uses four contacts on the sample periphery. By posing requirements on the sample geometry enough information can be obtained to extract the full in-plane resistivity tensor. Little literature exists on this, and all studies either assume the principal axis system of the resistivity tensor to be parallel to the edges of rectangular samples [22,23] or develop nonstandard measurement geometries [24–28]. The most successful of these methods adds a fifth contact and an additional resistance measurement to the vdP method [28].

This study focuses on expanding the theory of vdP measurements to extract the full in-plane tensor. The main focus is on single crystals where the principal axis system is fixed by crystal symmetry in most crystal classes. The knowledge of the principal axis system provides enough information to extract the tensor. A complimentary method is presented where the sample geometry is changed between two measurements. Together these methods allow extraction of the resistivity tensor in any anisotropic material where the tensor is constant

*Corresponding author: kasperab@chem.au.dk

 ©2015 American Physical Society

throughout the sample. By using only the standard vdP geometry, the techniques are more easily applied to measurements using commercial setups. The requirements for the sample geometry are relaxed from rectangles to parallelograms. The only additional measurement is the angle of the parallelogram. This is particularly useful in single crystals where the sample size is often limited. The theory developed for parallelogram shaped samples is directly applicable to the five-point method [28]. The theory and methods developed herein are thoroughly tested experimentally and numerical error simulations are discussed. Both methods are applied to the crystallographic (a,b) plane of a $RuSb_2$ single crystal. To the knowledge of the authors, only the resistivity of polycrystalline materials and along the crystallographic c axis has been reported.

II. THEORY

In the van der Pauw method, the four contacts A through D are placed in order along the circumference of an arbitrarily shaped disk without any holes. The resistance R_1 is measured by passing current between contact A and B (or C and D) and measuring the voltage between the remaining contacts, see Fig. 1. The resistance R_2 is equivalently measured by passing current between A and D (or B and C). These resistances fulfill the van der Pauw equation [19,20]

$$\exp\left(-\frac{\pi d R_1}{\rho}\right) + \exp\left(-\frac{\pi d R_2}{\rho}\right) = 1. \tag{1}$$

ρ is the resistivity and d is the sample thickness. Equation (1) can easily be proven for an infinite half-plane with contacts along the edge and the general case follows from the existence of a conformal mapping from the infinite half-plane to arbitrarily shaped surfaces without holes.

The vdP method distinguishes itself from the four-point bar method by being a two-dimensional (2D) technique independent of geometry. The sample thickness d enters to relate the three-dimensional (3D) resistivity to the 2D sheet resistance. In the bar method a resistance measurement is

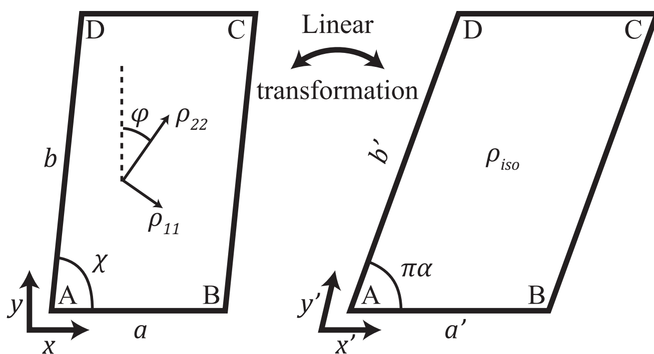

FIG. 1. Effect of the change of coordinates on the sample geometry and tensor. The sample (left) is anisotropic while the transformation results in an equivalent isotropic representation (right). φ is the angle between the tensor principal axis system and the laboratory axes. Before the transformation the laboratory axes are defined with x along the AB side and y perpendicular to this in the AD direction. χ is the angle in the anisotropic parallelogram while $\pi\alpha$ is the angle in the isotropic parallelogram.

combined with a known geometry to obtain the resistivity. In the vdP method, the geometry is substituted for a second, independent resistance measurement.

In a general anisotropic crystal, the resistivity turns into a tensor property with up to six independent elements. To measure the full tensor using bar samples, six bars with different orientations are needed. These bars cannot form a single plane and any two of them cannot be collinear. van der Pauw showed that the same approach is possible using arbitrarily shaped disks; here the normal vectors can also not form a single plane and any two cannot be collinear [29]. If the vdP method is performed on a sample with known geometry, Eq. (1) is over determined and only one resistance measurement is necessary, as in the bar method. If the sample is anisotropic this extra information can be used to reduce the number of required samples as two tensor elements can be determined per measurement. If the orientation of the in-plane principal axis system is known the full in-plane tensor can be determined (three elements). This is the case when two of the full 3D principal axes are in the sample plane and one is exactly perpendicular to this. If this is not the case, e.g., when one principal axis is not perpendicular to the plane or when the principal axis system of the full tensor is not known (i.e., when the axes are not fixed by crystal symmetry), the in-plane tensor can be extracted by performing a measurement on two sample geometries in the same plane. In practice this can be done by reshaping the sample (not a scaling) between the two measurements. How to relate the full tensor to the in-plane tensor is discussed in the Supplemental Material, Sec. S2 [30]. In the text only the in-plane tensor will be discussed from now.

To utilize this information, the sample geometry needs to be explicitly related to the complex half-plane where the resistances can be calculated, i.e., an explicit expression for the conformal mapping must be known. In this paper a parallelogram shaped sample is used, as this is often sufficient to maximize the sample surface area of planes of single crystals. The sample is mapped to the complex half-plane in two steps: First, a linear mapping from the anisotropic parallelogram to an equivalent isotropic parallelogram. Second, an explicit expression is used for the conformal mapping from the complex half-plane to the isotropic parallelogram. The explicit expressions for the two transformations allow the sample geometry to be related to the measured resistances and resistivity tensor elements. From these relations, the tensor elements can be calculated from measured quantities.

While a parallelogram is used here, other geometries can be used provided an expression for the conformal mapping to the isotropic equivalent geometry is known. The same steps used here to derive explicit expressions can be used for any geometry, both explicitly and numerically. The more quantities necessary to describe a sample geometry (angles and side lengths), the more complicated the expressions will generally be. Parallelograms result in complicated but reasonably tractable expressions; more complicated geometries would likely be easier to treat fully or partially numerically.

A last note is on the behavior in magnetic fields. In this case the total tensor becomes a sum of the magnetoresistivity (here taken to include the zero-field resistivity) and Hall resistivity tensor. The total tensor depends on the magnetic field direction and strength and hence becomes rank-3 (can no longer strictly

be represented as a matrix). As the magnetic field is often applied perpendicular to a flat sample, this can still be treated as a rank-2 tensor. However, it is important to realize that the tensor implicitly depends on the field direction. The Hall resistivity tensor for a given field direction is antisymmetric with zeroes on the diagonal and hence only has one element in a planar sample. The magnetoresistivity tensor is symmetric with nonzero diagonal elements. Experimentally, the two can be separated by the field dependence: The magnetoresistivity tensor is an even function of the magnetic field while the Hall resistivity tensor is an odd function of the field strength [18]. The contributions to a measured resistance from the two tensors can be experimentally separated by reversing the field direction or using the different reciprocity relations [3]. Without a magnetic field, interchanging the voltage and current contacts in a resistance measurement gives the same resistance (known as reciprocity). In a magnetic field, this causes the Hall effect contribution to change sign and hence the magnetic field will also need to be reversed (known as reverse field reciprocity) [31,32]. It should be noted that only the symmetric part of the tensor can be treated in the way presented here and will need to be separated from the antisymmetric part. The Hall resistivity part can be measured in the usual manner since there is only one in-plane element. In a magnetic field the full magnetoresistivity and Hall resistivity tensors can have up to 18 or 9 elements, respectively. For most inorganic compounds this is significantly reduced by the crystal symmetry.

As is the case for the Hall resistivity tensor, the Hall coefficient tensor will also be rank-3 and contain up to nine elements. The tensors are related through $R_{\mathrm{H}} = \rho_{\mathrm{H}} d/B$, where R_{H} is the Hall coefficient tensor, ρ_{H} is the Hall resistivity tensor, d is the sample thickness, and B is the magnetic field strength used in the measurement. This assumes all measurements to have been carried out at the same field strength. The Hall coefficient is often used to calculate the Hall carrier concentration to estimate the true carrier concentration. Since the Hall coefficient tensor in anisotropic materials can have up to nine independent and distinct values, so can the Hall carrier concentration. The true carrier concentration, however, is the number of electrons or holes in the conduction or valence bands, respectively. As such, it is a scalar number. The two carrier concentrations are related by $n = r_{\mathrm{H}} n_{\mathrm{H}}$, where r_{H} is the Hall factor, and n and n_{H} are the true and Hall carrier concentrations, respectively [33]. The Hall factor is a band structure property accounting for carriers in bands not behaving like a free electron gas. This property has a directional dependence and is described by a tensor. Thus, to avoid discrepancies between reports, it is important to carefully describe the methodology employed when reporting Hall carrier concentrations of anisotropic samples.

A. Isotropic equivalent sample

To relate the resistivity tensor to the sample geometry and measured resistances, the Laplace equation for the sample must be solved. To simplify this, the sample is mapped to the upper complex half-plane where the resistances can be easily calculated. While this can be done directly using a conformal mapping, this would result in the tensor not being constant on the complex half-plane, thus complicating the calculations. By first mapping the anisotropic sample linearly to an equivalent isotropic sample, this problem is removed. For reference, this transformation is applied to the Laplace equation in the Supplemental Material, Sec. S1 [30]. Here only the result is used.

A sample shaped as a parallelogram with angle χ and side lengths a and b will be used. Its resistivity is given by the symmetric tensor $\rho = \begin{pmatrix} \rho_{xx} & \rho_{xy} \\ \rho_{xy} & \rho_{yy} \end{pmatrix}$, which is the most general case in two dimensions without a magnetic field. The principal axis system of the tensor is rotated by φ (in the negative direction) relative to the laboratory frame. This is illustrated in the left of Fig. 1. If the orientation is known the tensor in the laboratory frame can be expressed in terms of its components ρ_{11} and ρ_{22} along the principal axes $\boldsymbol{e}_1$ and $\boldsymbol{e}_2$. This will be further explored later.

The transformation is done by the matrix

$$\mathrm{M} = \frac{1}{\sqrt{\rho_{yy}\rho_{\mathrm{iso}}}} \begin{pmatrix} \rho_{yy} & -\rho_{xy} \\ 0 & \rho_{\mathrm{iso}} \end{pmatrix}. \tag{2}$$

The definition $\rho_{\mathrm{iso}} = \sqrt{\det \rho} = \sqrt{\rho_{xx}\rho_{yy} - \rho_{xy}^2}$ has been used. When applying this to the Laplace equation, the transformation rule $\rho' = M\rho M^{\mathrm{T}}$ is found to apply to the resistivity tensor (see Supplemental Material, Sec. S1 [30]) and results in $\rho' = \begin{pmatrix} \rho_{\mathrm{iso}} & 0 \\ 0 & \rho_{\mathrm{iso}} \end{pmatrix}$. The transformation results in an isotropic representation of the sample with resistivity ρ_{iso}. The sample geometry is transformed by transforming the vectors representing the sample $\boldsymbol{a}$ and $\boldsymbol{b}$ sides to $\boldsymbol{a}' = M\boldsymbol{a}$ and $\boldsymbol{b}' = M\boldsymbol{b}$. These are both nonstandard transformation rules, which result from the change of variables in the Laplace equation. After the transformation, the new side lengths are

$$a' = a\sqrt{\frac{\rho_{yy}}{\rho_{\mathrm{iso}}}}, \tag{3}$$

$$b' = b\sqrt{\cos^2(\chi)\frac{\rho_{yy}}{\rho_{\mathrm{iso}}} + \sin^2(\chi)\frac{\rho_{xx}}{\rho_{\mathrm{iso}}} - 2\cos(\chi)\sin(\chi)\frac{\rho_{xy}}{\rho_{\mathrm{iso}}}}. \tag{4}$$

The angle between a' and b' is defined by

$$\cos(\pi\alpha) = \frac{1}{\sqrt{\rho_{yy}}} \frac{\cos(\chi)\rho_{yy} - \sin(\chi)\rho_{xy}}{\sqrt{\cos^2(\chi)\rho_{yy} + \sin^2(\chi)\rho_{xx} - \cos(\chi)\sin(\chi)\rho_{xy}}}. \tag{5}$$

Equations (3) to (5) are derived in the Supplemental Material, Sec. S3.a [30]. Since the change of variables was applied to the Laplace equation, either representation of the sample can be used to calculate or measure the electrostatic potential. Any measurement performed on one sample would give the same result if performed on the other, provided the contact placement is also transformed correctly. As a consequence, a normal vdP resistivity measurement performed on an anisotropic sample will result in ρ_{iso}.

In a magnetic field, ρ becomes the magnetoresistivity tensor and these elements are used to define M from Eq. (2). Applying

the transformation to the antisymmetric Hall resistivity tensor does not change the tensor, i.e., $M\rho_H M^T = \rho_H$. This further underlines the equivalence of performing measurements on the two samples.

B. Conformal mapping

In the original derivation of the vdP equation [19,20], the existence of a conformal mapping between some 2D areas and an infinite half-plane was used. The criterion of physical interest is that the outline of the area has to be singly connected, which is to say there can be no isolated holes in the area. A conformal mapping is any mapping that locally preserves angles while distances are not necessarily conserved. van der Pauw did not need an explicit expression for the mapping since the contact placement on the infinite half-plane vanishes from the vdP equation. Here an explicit expression is necessary since the information contained in the sample geometry is needed to extract more information from the measured resistances.

Figure 2 illustrates the conformal mapping defined by the equation [24,26]

$$\xi' = w(\xi) = \frac{a'}{A_{\alpha,k}} \int_0^{\xi} f_{\alpha,k}(z)dz, \tag{6}$$

where

$$f_{\alpha,k}(z) = z^{\alpha-1}(1-z)^{-\alpha}(1-kz)^{\alpha-1} \tag{7}$$

and

$$A_{\alpha,k} = \int_0^1 f_{\alpha,k}(z)dz = \Gamma(\alpha)\Gamma(1-\alpha)\,{}_2F_1(1-\alpha,\alpha;1;k). \tag{8}$$

$w(\xi)$ takes a point $\xi = x + iy$ on the half-plane and maps it to a point (x', y') in the isotropic parallelogram. The point is represented by the complex number $\xi' = x' + iy'$. α is the angle in radians of the isotropic parallelogram divided by π. k^{-1} is the position of contact C along the real axis on the half-plane. Γ and ${}_2F_1$ are the Gamma function and Gaussian hypergeometric function, respectively.

k and α can be related to the geometry of the isotropic equivalent sample by considering the length of the mapped BC side. This can be calculated from the conformal mapping

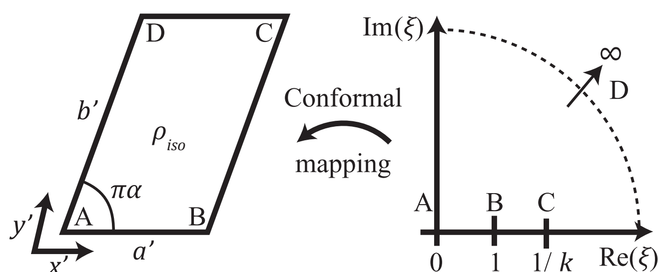

FIG. 2. Illustration of the conformal mapping with contact placements. Contact D corresponds to infinity in any direction on the upper complex half-plane. k has to be in the range $0 < k < 1$ for contact C to be placed between contacts B and D.

as [27,34]

$$b' = \frac{a'}{A_{\alpha,k}} \int_1^{k^{-1}} f_{\alpha,k}(z)dz = \frac{a' A_{\alpha,1-k}}{A_{\alpha,k}}. \tag{9}$$

$A_{\alpha,k}$ is a normalization constant and in the following only ratios such as in Eq. (9) will appear. Hence it is convenient to define

$$B_{\alpha,k} = \frac{A_{\alpha,1-k}}{A_{\alpha,k}} = \frac{{}_2F_1(\alpha,1-\alpha;1;1-k)}{{}_2F_1(\alpha,1-\alpha;1;k)}. \tag{10}$$

This can easily be calculated using standard mathematical software such as MATLAB™ or from an infinite series (see Supplemental Material, Sec. S4.a [30]).

The infinite (complex) half-plane provides a system that allows easy calculation of the electrostatic potential differences between the contacts when a current is passed through the sample. As no scaling is performed, the resistivity of the infinite half-plane sample is still ρ_{iso}. $R_{\text{AB,DC}}$ denotes the ratio of the voltage between contact D and C when a current is passed from A to B. In a vdP measurement including Hall effect, three such resistances are measured:

$$R_{\text{AB,DC}} = \frac{U_D - U_C}{I_{\text{AB}}} = \frac{-\rho_{\text{iso}}}{\pi d} \ln(1-k), \tag{11}$$

$$R_{\text{BC,AD}} = \frac{-\rho_{\text{iso}}}{\pi d} \ln(k), \tag{12}$$

$$R_{\text{AC,BD}} = \frac{-\rho_{\text{iso}}}{\pi d} \ln(k^{-1} - 1). \tag{13}$$

d is the sample thickness. The derivation can be found in the Supplemental Material, Sec. S3.b [30], and is done in the absence of magnetic fields. These are mutually dependent and one measurement is enough to determine k while α cannot be obtained from these resistance measurements. The resistance in Eq. (13) [which is the difference between the resistance in Eqs. (11) and (12)] corresponds to the Hall effect measurement and is a resistive offset to the Hall signal. Both resistances in Eqs. (11) and (12) are necessary for the vdP measurement and are used to calculate ρ_{iso} from the vdP equation. Equation (13), however, provides no new information.

Since the Hall resistivity tensor only contributes a voltage perpendicular to the current direction, and no current can flow perpendicular to the sample edge at the edge, a voltage measurement between two consecutive contacts will not be affected by the Hall effect. Hence, since the method presented here only relies on the resistances in Eqs. (11) and (12), this is directly applicable to the magnetoresistivity tensor. The Hall effect will add a contribution of ρ_{xy}^{H}/d to Eq. (13), where ρ_{xy}^{H} is the off-diagonal element of the Hall resistivity tensor for the sample. This assumes the magnetic field points out of the sample plane as defined in Figs. 1 and 2. The contribution to $R_{\text{BD,AC}}$ will be equal but with opposite sign, and both contributions will change sign if the magnetic field is reversed.

C. Calculating the tensor elements

After the measurement ρ_{iso} and k are known but no information on α is obtained. Determining α will be the focus of the following sections. Using the definition for ρ_{iso} together

with Eqs. (3)–(5) and (9) the tensor elements can be expressed in terms of α and known parameters

$$\rho_{xx} = \frac{1}{\sin(\chi)} r B_{\alpha,k}\lambda_\alpha + \frac{\cos(\chi)}{\sin(\chi)}\lambda_\alpha\left[\cos(\chi)r^{-1}B^{-1}_{\alpha,k} - 2\cos(\pi\alpha)\right], \quad (14)$$

$$\rho_{yy} = \sin(\chi)r^{-1}B^{-1}_{\alpha,k}\lambda_\alpha, \quad (15)$$

$$\rho_{xy} = \cos(\chi)r^{-1}B^{-1}_{\alpha,k}\lambda_\alpha - \lambda_\alpha\cos(\pi\alpha). \quad (16)$$

$r = a/b$ is the ratio of the anisotropic sample a and b sides and $\lambda_\alpha = \rho_{\text{iso}}/\sin(\pi\alpha)$. The derivation of Eqs. (14)–(16) is quite lengthy and can be found in the Supplemental Material, Sec. S3.c [30].

Initially, simply assuming $\pi\alpha = \chi$ provides useful information. The assumption is equivalent to assuming the principal axis system to be identical to the laboratory frame $\varphi = 0$. The estimated anisotropy (ratio of ρ_{11} to ρ_{22}) from this will never be further from 1 than the true anisotropy and can thus be used as a limit. If the sample is anisotropic it is still possible, but unlikely, that the sample will be found to be isotropic. This will only happen for $\varphi = 45^\circ$.

1. Known principal axis system

In single crystals, the orientation of the crystallographic axes can be determined using standard diffraction techniques. In all crystal classes except triclinic and monoclinic this also implies knowledge of the principal axes orientation (see Supplemental Material, Sec. S2, for a discussion [30]) and hence φ is known, if two principal axes are in the sample plane. The tensor can then be expressed in terms of the elements along the principal axes and the orientation as $\rho = (R^\varphi)^{\mathrm{T}}\rho_0 R^\varphi$. ρ_0 is the tensor in the principal axis system which has only diagonal elements and R^φ is the matrix rotating vectors φ in the positive direction (see Supplemental Material, Sec. S1 [30]). Now only two tensor elements need to be determined. This can be combined with Eqs. (14)–(16) to give an equation relating α to measured parameters:

$$0 = \left(\frac{1}{\tan(2\chi)} + \frac{1}{\tan(2\varphi)}\right)2\cos(\chi)r^{-1}B^{-1}_{\alpha,k} + \frac{1}{\sin(\chi)} r B_{\alpha,k} - \left(\frac{1}{\tan(\chi)} + \frac{1}{\tan(2\varphi)}\right)2\cos(\pi\alpha). \quad (17)$$

This equation can be solved to get α. The derivation can be found in the Supplemental Material, Sec. S3.d [30]. In some cases, the equation may have two solutions which both result in valid but different tensors. This occurs when the parameters (φ, χ, k, and r) lie close to a region in the parameter space that does not correspond to any physically valid situation. Experimental noise in the parameters may shift them into the region without any solutions. This is further discussed in the Supplemental Material, Sec. S4.a [30].

The equation needs to be solved numerically. A MATLAB™ script for this can be supplied by contacting the corresponding author. Once α has been obtained the tensor in the laboratory frame can be calculated from Eqs. (14)–(16) and the principal elements can be obtained by a rotation of the laboratory frame tensor. An algorithm for solving Eq. (17) is found in the Supplemental Material, Sec. S4.a [30].

2. Unknown principal axis system

If the orientation of the tensor elements is not known more information needs to be obtained by other means. This could be when the principal axis system is not fixed by crystal symmetry, the sample is not perpendicular to a principal axis, or the crystallographic orientation is unknown. It is possible to perform a five-point analog to the vdP measurement [27], however, this requires modification of the measurement system. This is not easily done with commercial systems but custom setups may be more easily adapted to accommodate a fifth contact [21]. The five-point method can be directly combined with the theory in this work.

If such modification is not feasible extra information can be obtained by modifying the sample, as indicated in Fig. 3. An initial measurement is performed (middle sample, called A), the sample geometry is changed, and a second measurement is performed (such as on the left or right samples, called B). If the sample is homogenous the tensors in A and B are identical except for possibly a rotation. If ρ_{iso} changes more than a few percent the sample is most likely inhomogeneous or other errors are affecting the measurement. After the measurement on A, the parameters r_A, k_A, χ_A, and ρ_{iso} are known and the tensor can be calculated as a function of only α, $\rho(\alpha)$. In B these parameters are different but still known and the tensor principal axis system has been rotated by θ (which may be negative, zero, or positive). The new tensor $\rho'(\beta,\theta)$ expressed in the A reference frame can hence be calculated as a function of the new α, now called β, and θ.

Rotating the tensor in B by $-\theta$ will result in the same tensor as in A. This gives the equation

$$\rho(\alpha) = \rho'(\beta,\theta) = (R^\theta)^T\rho(\beta)R^\theta. \quad (18)$$

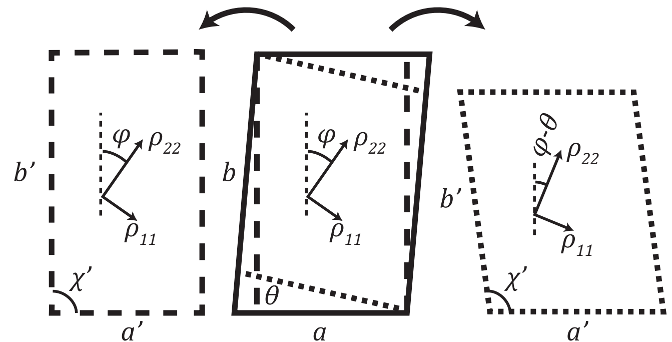

FIG. 3. Reshaping the sample between two measurements can provide enough information to determine α. After the first measurement the middle sample is cut along either the dotted or dashed lines. In the right sample with the dotted line the tensor principal axes has been rotated relative to the lab frame, indicated by the angle θ. In the left sample, the sample geometry has changed but the tensor principal axes have the same orientation. The sample can be reshaped in many more ways which will give the right result provided attention is paid to the rotation of the tensor principal axes.

This corresponds to three equations, one for each of the tensor elements. To solve this, the vector

$$d(\alpha,\beta) = \begin{pmatrix} \rho_{xx}(\alpha) \\ \rho_{yy}(\alpha) \\ \rho_{xy}(\alpha) \end{pmatrix} - \begin{pmatrix} \rho_{xx}(\beta,\theta) \\ \rho_{yy}(\beta,\theta) \\ \rho_{xy}(\beta,\theta) \end{pmatrix} = 0 \qquad (19)$$

is used to reduce the system of equations to one equation. Equation (19) can then be solved by finding the minimum in $d^2(\alpha,\beta)$. This can be solved using Newton's method or the method of steepest descent. A discussion of this is found in the Supplemental Material, Sec. S4.b [30], and a MATLAB™ script can be supplied by contacting the corresponding author. This method is equivalent to van der Pauw's approach but with the extra information on the sample geometry taken into account.

It is not necessary to change χ for the method to work and θ may also be 0. A change in r alone is sufficient. Any modification of the sample except a scaling is acceptable. The fundamental criterion is that at least one of the parameters determining ρ are changed, that is χ, k, or r. If the sample is simply scaled, any value of $\alpha = \beta$ will solve Eq. (19).

D. Numerical error analysis

An important source of error is the contact placement. If the contacts are not placed exactly on the corners, errors in the tensor elements are expected while ρ_{iso} is not expected to change. Finding a general analytic expression for the error from misplaced contacts is difficult. Instead, it can easily be simulated numerically by moving a contact on the complex half-plane away from the correct position and mapping this to the sample using the two transformations in Eqs. (6) and (2). As with the normal vdP method, small errors from several misplaced contacts are expected to be additive [19,20].

The A and C as well as B and D corners of the sample are mathematically identical and give the same error for contact displacements. Considering only the distinct A and B corners is hence sufficient. An example of an error simulation of the two distinct corners is shown in Fig. 4. The angles of the corresponding corners of the isotropic equivalent sample are noted in the figure. The error in each corner is calculated for displacements towards both adjacent corners, as noted. For the calculations a tensor with principal axis elements $\rho_{11} = 1$ and $\rho_{22} = 2.73$ (arbitrary units) and orientation $\varphi = 54.08^\circ$ was used. The sample had aspect ratio $r = 1$ and angle $\chi = 90^\circ$. This was chosen as it corresponds to a sample used later in this paper. The calculated change in tensor elements when moving a contact was divided by ρ_{iso} since this sets the scale for the tensor elements. If the change is calculated relative to the individual elements errors in elements with low values are overemphasized.

From the figure it is seen that the error in corners with high angle (in the isotropic equivalent sample) is significantly larger than in low angle corners and hence these should be avoided, i.e., it is recommended to keep α close to 0.5. This is a more general requirement than can be made for the anisotropic sample itself since the current paths will depend strongly on the tensor. Keeping the error in contact placement less than a few percent is possible even for small samples and the total error from this source are expected to be less than 3%–5% of ρ_{iso}.

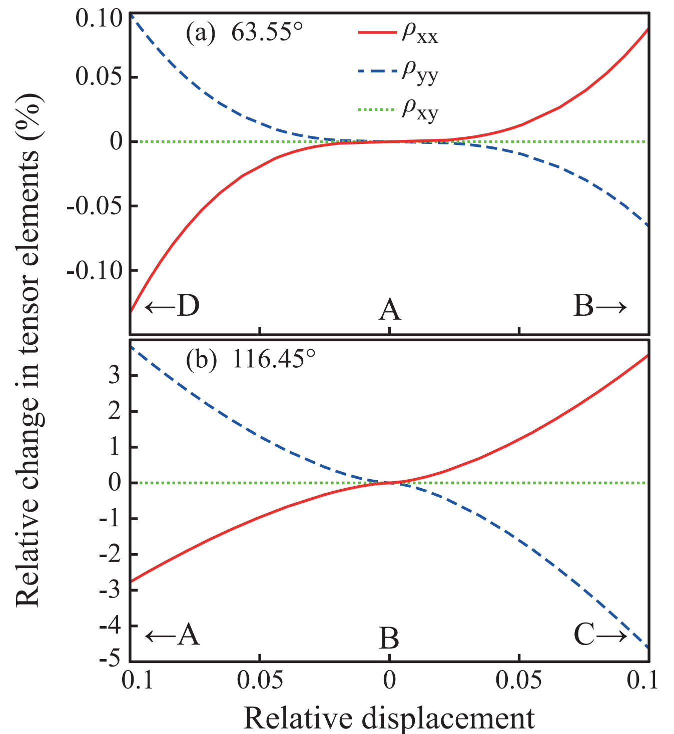

FIG. 4. (Color online) Tensor element error relative to ρ_{iso} for displacement of the A (a) and B (b) contacts toward the adjacent corners. The displacement is relative to the a and b side lengths.

Another source of error is from the angles in the parallelogram, either errors in χ or deviations from a parallelogram towards a trapezoid or general quadrilateral. Errors in χ can easily be simulated numerically while the later has to be tested experimentally since the conformal mapping no longer holds (another expression is needed).

A simulation of the error as a function of the error in χ is shown in Fig. 5. The error from χ is less sensitive to the angle of the corner in the isotropic equivalent than for contact displacements. The angle of the sample can be measured with high accuracy with a digital microscope or equivalent and the error will usually not exceed 0.5°. Hence, the error from measuring the angle is expected not to exceed 1%–2% of ρ_{iso}.

The errors from χ in the two corners are related but not identical. The sample has been rotated 90°, thus interchanging ρ_{xx} and ρ_{yy} and changing sign of ρ_{xy}. Additionally, a positive error in (a) corresponds to a negative error in (b). If the x axis in (b) is inverted and the sign of the error in ρ_{xy} is changed the two plots are very similar. They are only completely identical for isotropic, square samples due to the 90° rotation.

Apart from these errors, the requirements for the vdP method still apply: The sample has to be flat, of uniform thickness, and there can be no holes. For round samples it has been found that samples can be considered flat if the thickness is less than the radius [35]. Extending this to other geometries is not trivial; however, keeping the thickness well below the shortest distance across a sample and between any two contacts

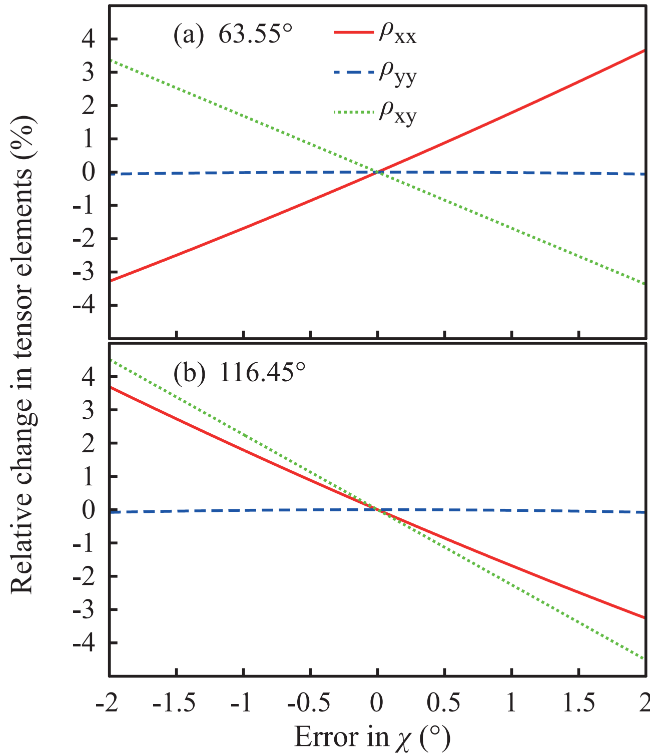

FIG. 5. (Color online) Relative change in tensor elements as a function of error in χ. The simulation was carried out using the same sample as in Fig. 4, and normalized with ρ_{iso}.

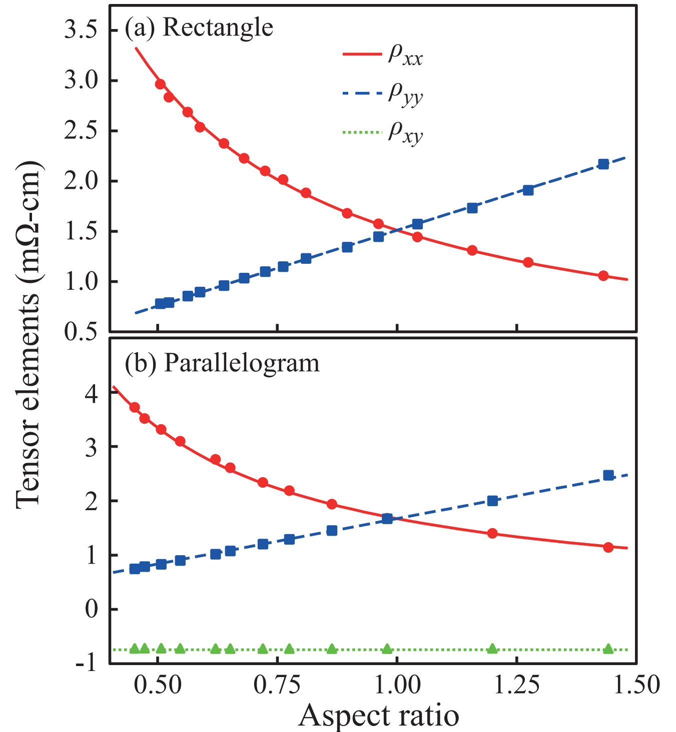

FIG. 6. (Color online) Tensor elements as a function of aspect ratio of the isotropic equivalent sample. The points are from the measured resistances and the lines are calculated from the aspect ratio and average resistivity. The graphite was shaped as a rectangle in (a) and as a parallelogram with $\pi\alpha$ corresponding to 63.55° in (b).

should provide a reasonable rule of thumb. When this limit is approached a more accurate estimate is required, which can be acquired from an experimental test or numerical simulation.

MATLAB™ scripts for performing the numerical error analysis presented here can be supplied by contacting the corresponding author.

III. EXPERIMENTAL TEST ON ISOTROPIC GRAPHITE

Several test systems were employed to test the rigidity of the theory and assess experimental noise. All geometric parameters were measured ten times. Angles were measured with a digital microscope and dimensions were measured with a micrometer with 10 μm delimitation. The standard deviation never exceeded 0.5° for angles and 40 μm for dimensions. Generally, deviations were below 0.15° and 10 μm, respectively. To ensure all samples could be considered flat, the thickness never exceeded 1/3 of the shortest side length.

To test the validity of the conformal mapping and measurement precision, pseudoanisotropic samples were prepared. Polycrystalline graphite with close to isotropic resistivity was shaped as the isotropic equivalent of an imagined anisotropic sample. The tensor was then independently calculated from (1) the measured resistances and (2) using only the geometry of the graphite. This allows testing of the conformal mapping since (2) depends only on sample geometries and ρ_{iso} (average of all measurements on each sample) while (1) also relies on the conformal mapping. To simulate different degrees of anisotropy the aspect ratio of the graphite was progressively increased in small steps from about 0.5 to about 1.5. This changes k, while angles were kept fixed. Figure 6 shows the tensor elements from (1), shown as points, compared to (2), shown as lines. As seen in Fig. 6, there is a good agreement between the tensor elements from the two methods, supporting the conformal mapping approach.

Two samples were used for this test: One was a rectangle with $\alpha = 0.497$ and the other was a parallelogram with $\alpha = 0.353$. In both cases the imagined anisotropic sample was assumed to have $\chi = 90°$ and $r = 1$.

A. Reproducibility and errors

The reproducibility was tested by mounting and measuring two graphite samples 20 times each. These samples were the graphite samples used for Fig. 6 with $r = 0.81$ (rectangle) and $r = 0.86$ (parallelogram). The samples were rotated between measurements, resulting in continued cyclic permutation of the contacts. This ensures low correlation of errors between successive measurements. From this two types of errors can be calculated: a parallel shift of the elements corresponding to an error in ρ_{iso} and an antiparallel shift of ρ_{xx} and ρ_{yy} corresponding to an error in geometry. The latter error is most likely from bad contact placement. The errors relative to ρ_{iso} (average of all measurements on each sample) are shown in Fig. 7. The ρ_{iso} error is seen to be much smaller than the geometric error. This is expected since the vdP resistivity measurement is precise while accurate contact placement is

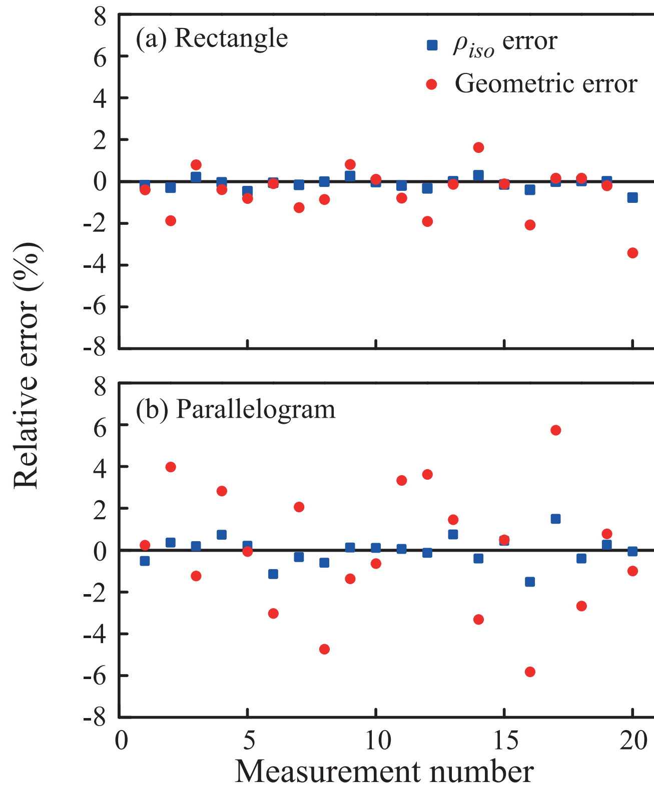

FIG. 7. (Color online) Errors in tensor elements relative to ρ_{iso} for 20 repeated measurements. The graphite was shaped as a rectangle in (a) and as a parallelogram with $\pi\alpha$ corresponding to 63.55° in (b) with aspects ratios $r = 0.81$ and $r = 0.86$, respectively.

difficult. The vdP resistivity measurement is not affected by contact positions as long as they are on the sample edge.

The errors are three times larger for the parallelogram than the rectangle. This is due to a combination of $\pi\alpha$ being far from 90° and that parallelograms are slightly harder to mount correctly. The error is the deviation from the tensor elements calculated from the geometry and average resistivity divided by ρ_{iso}. This corresponds to the lines in Fig. 6. The errors shown in Figs. 4 and 5 were calculated for the sample used in Fig. 7(b). Assuming errors up to 5% on the contact placement and 0.5° in χ, the expected maximum error of roughly 6% fit well with that observed in Fig. 7(b). The 6% estimate is obtained by adding roughly 2% for the B and D contacts, negligible contribution from the A and C contacts, and 2% from χ. The same error analysis for the sample in Fig. 7(a) gives a 2% error which is similar to the scatter observed in the figure. This indicates that these error plots give good estimates of the expected maximum error in the method, provided the vdP method is correctly and carefully applied.

A type of error, which cannot easily be estimated by numerical simulations, is deviation from parallelograms towards a trapezoid, i.e., opposing sides not being completely parallel. In this case the expression for the conformal mapping is no longer valid. The effect of this error was tested on a graphite sample with $\chi = 90.27°$ and $r = 0.996$. The angle between two opposing sides was progressively increased by grinding away wedges of one side. The change in the tensor elements

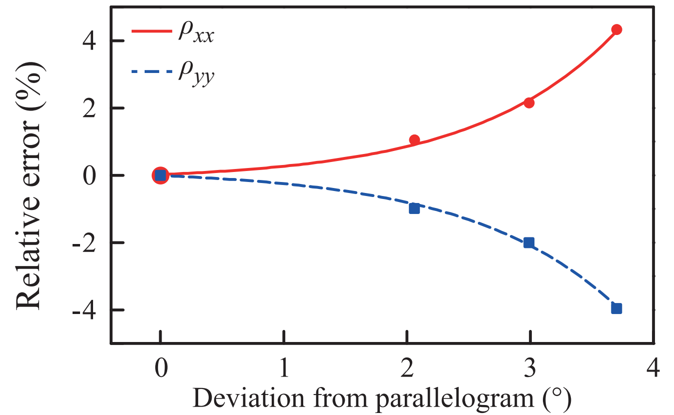

FIG. 8. (Color online) Error in tensor elements relative to ρ_{iso} as a function of deviation from a parallelogram in degrees. The lines are guides to the eye.

relative to ρ_{iso} was calculated. This error is plotted against the measured deviation in Fig. 8. Ensuring parallel sides in a parallelogram poses little practical challenge and this deviation is usually expected to be much less than 1°. Hence, the error from this effect is expected to be less than 1% if appropriate care is taken.

B. Using two samples

Graphite was also used to test the extraction of α from Eq. (19). A rectangular piece of graphite was shaped in five steps into a progressively more skewed parallelogram. Measurements were performed on all samples and all unique combinations of the five measurements were used to extract α from Eq. (19) and calculate the tensor elements. The results can be seen in Fig. 9. The reference frame is the same in all samples (i.e., $\theta = 0$) since the AB side was unchanged.

If the two samples are too similar, Eq. (19) will have a flat minimum. In this case, the algorithm for solving the equation converges slower. The low gradient also increases the effect of experimental noise on α and the tensor elements.

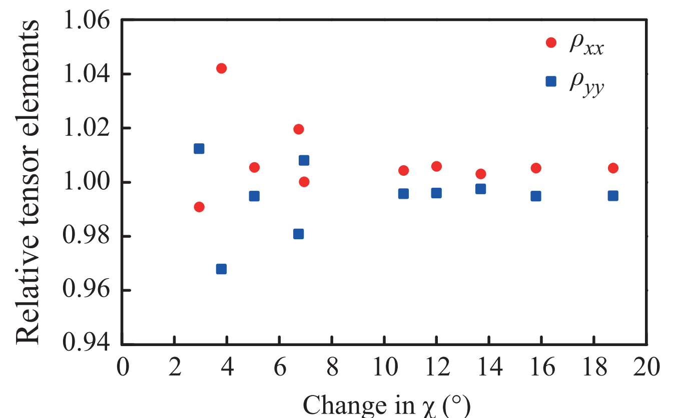

FIG. 9. (Color online) Tensor elements divided by ρ_{iso} as a function of the change in χ in the parallelogram. α was extracted from Eq. (19). While ρ_{xy} is not strictly 0 this is omitted since it is small and has a low variation.

Determining the minimum change in χ required for the effect of experimental noise to be tolerable is not straightforward. In most cases, a change of 15° or more should suffice and not pose major practical problems.

IV. $RuSb_2$ SINGLE CRYSTAL

An approximately 20 mm^3 $RuSb_2$ single crystal was grown from an antimony self-flux. The starting material was a mixture of 3.4161 g small $RuSb_2$ crystals from a previous synthesis, 0.2168 g Ru (99.9% metals basis), and 22.9863 g Sb (99.9999% metals basis) and was placed in an Al_2O_3 crucible in a quartz ampule. This gives a roughly 6:94 molar Ru:Sb ratio. The ampule was sealed at a pressure of less than 10^{-4} mbar and placed inside an Al_2O_3 tube filled with thermally insulating ceramic wool. The insulated ampule was heated to 1100 °C at 150 K/h and soaked for 5 h, cooled to 640 °C at 1 K/h, after which the furnace was turned off. To remove the excess flux, the crucible was placed upside down in another ampoule with ceramic wool (collects the solid) on top of quartz shards (provides a reservoir for the flux) in the bottom. This ampule was heated to approximately 690 °C for 30 min and centrifuged while hot. While heating and centrifuging, the ampoule was placed in a special high thermal mass and insulated stainless steel receptacle to prevent the flux from solidifying before the centrifugation had completed. The synthesis produced crystals at a variety of sizes, some of which were agglomerated. The largest isolated crystal with well-defined facets on all sides was selected for the experiments. The facets were indexed in a powder x-ray diffractometer and the angles between the facets were consistent with a single crystal. $RuSb_2$ has the marcasite structure (space group *Pnnm*) with lattice constants of $a = 5.95$ Å, $b = 6.67$ Å, and $c = 3.18$ Å [36].

From the single crystal a parallelogram in the (a,b) plane was cut. This sample had $r_A = 0.705$, $\chi_A = 96.2°$, and $\varphi_A = 45.7°$. The measurement resulted in $\rho_{iso} = 101$ mΩ cm and $k = 0.116$. When Eq. (17) is solved with this input, two values of α result: 0.128 and 0.659. This results in the two tensors $\begin{pmatrix} 562 & 0 \\ 0 & 18.3 \end{pmatrix}$ and $\begin{pmatrix} 66.9 & 0 \\ 0 & 154 \end{pmatrix}$ mΩ cm. The first solution indicates the b direction to be more resistive and the second solution indicates the a direction to be more resistive. In this sample this cannot be used to determine the correct solution; however, this may be possible in some samples such as layered compounds.

To distinguish the two solutions, a new sample with a geometry defined by $r_B = 0.957$, $\chi_B = 79.6°$, and $\varphi_B = 62.3°$ was cut from the first. The two samples are related by $\theta = -16.6°$. From the measurement $\rho_{iso} = 116$ mΩ cm and $k = 0.287$ was obtained. Only one α, 0.553, is obtained from the single crystal equation. This results in the tensor $\begin{pmatrix} 78.7 & 0 \\ 0 & 170 \end{pmatrix}$ mΩ cm. From this it seems likely that the second solution in the first sample is the correct one even though they differ somewhat. This is due to a 15% increase in ρ_{iso} between the two measurements. The anisotropy, defined as ρ_a/ρ_b, is 2.29 in the first sample second solution and 2.16 in the second sample. This corresponds to less than 6% decrease in anisotropy, much less than the change in ρ_{iso}. The reason for the lower resistivity in the first sample is most likely bad measurements due to, e.g., excessively large contacts, contacts not being on the circumference, etc. These errors all result in a decrease in measured resistivity [19,20]. Repeated measurements on the second sample gave comparable results.

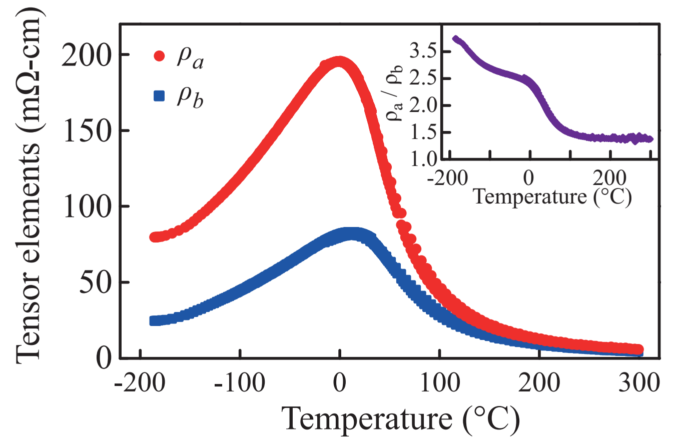

FIG. 10. (Color online) Temperature resolved measurement of ρ_a and ρ_b of $RuSb_2$. The single crystal method and Eq. (17) with constant, temperature independent φ were used. The inset shows ρ_a/ρ_b.

The method of changing the sample geometry can strictly not be applied due to the change in resistivity. Nonetheless, this is included for comparison. Using $\rho_{iso} = 109$ mΩ cm (average of the two samples) gives $\alpha = 0.639$ and $\beta = 0.540$, which is similar to the values obtained from the single crystal method. This results in the tensor $\begin{pmatrix} 76.7 & 0 \\ 0 & 154 \end{pmatrix}$ mΩ cm and anisotropy 2.00. Despite the large change in ρ_{iso} the tensor is quite similar to the ones calculated from the single crystal method. This is expected since both k and α depend on the anisotropy rather than the actual resistivity. Since the anisotropy only changes slightly, k and the extracted α and β are still reasonably accurate.

The second sample was used to measure the resistivity from −185 to 300 °C. The data are shown in Fig. 10. Since the unit cell orientation is independent of temperature, φ is constant during temperature resolved measurements. This allows for easy application of the single crystal method to temperature resolved measurements.

The resistivity has a metallic region at low temperatures and shows activated behavior at higher temperatures. The temperature dependence below 100 °C is similar to that reported by Sun *et al.* [6] along the c direction. Fitting an Arrhenius type expression to the activated region (75–300 °C) gives a thermal band gap of 0.34 eV, consistent with previously reported values. Below −185 °C another activated region has been reported [6], the onset of which is visible as a positive curvature in resistivity. Hall coefficient measurements (not shown) indicate an n- to p-type transition at 30 °C. Below this temperature the material is n type.

The anisotropy seems to stabilize at around 1.4 and is almost independent of temperature above 150 °C. This indicates that the relative mobility of the a and b directions is constant. In conventional semiconductors this ratio is mainly determined by the Fermi surface. Hence, the conduction band Fermi surface has a constant shape from 150 to at least 300 °C. The anisotropy increases at lower temperatures and reaches a plateau in the low temperature metallic region. Another

increase is observed when the low temperature activated region is approached. This and previously published Hall effect data support at multiband model with at least three bands. The low temperature activated region is likely due to excitation of impurity states [6], while the high temperature excited region is due to the conduction band becoming dominant due to thermal excitation across the band gap.

V. CONCLUSION

The theory of the van der Pauw method has successfully been extended to extract the resistivity tensor of single crystals. Two methods for extracting the in-plane resistivity tensor have been presented. One uses the orientation of the crystallographic axes to determine the tensor while the other requires reshaping a sample between two measurements. Tests on graphite samples indicate the theory to be consistent and the precision to be high. Numerical error simulations further support this conclusion. Applying both methods to a $RuSb_2$ single crystal gives comparable results and allows easy extraction of the resistivity along the *a* and *b* directions from a single temperature resolved measurement. The methods are concluded to have good precision and be easy to implement.

ACKNOWLEDGMENTS

The work was supported by the Danish National Research Foundation, Grant No. DNRF93 (Center for Materials Crystallography, DNRF93). K.A.B. is thankful for funding from the Danish Council for Independent Research (DFF), Grant No. 4090-00071, and the DFF Sapere Aude program. D.R.B. would like to acknowledge the support of the Resnick Sustainability Institute.

[1] S. R. De Groot and P. Mazur, *Non-equilibrium Thermodynamics* (Dover, New York, 1984).
[2] J. F. Nye, *Physical Properties of Crystals* (Oxford University Press, Oxford, 1985).
[3] K. A. Borup, J. de Boor, H. Wang, F. Drymiotis, F. Gascoin, X. Shi, L. Chen, M. I. Fedorov, E. Muller, B. B. Iversen, and G. J. Snyder, Energy Environ. Sci. **8**, 423 (2015).
[4] G. J. Snyder and E. S. Toberer, Nat. Mater. **7**, 105 (2008).
[5] A. Bentien, S. Johnsen, G. K. H. Madsen, B. B. Iversen, and F. Steglich, Europhys. Lett. **80**, 17008 (2007).
[6] P. Sun, N. Oeschler, S. Johnsen, B. B. Iversen, and F. Steglich, J. Phys. Conf. Ser. **150**, 012049 (2009).
[7] L. E. Bell, Science **321**, 1457 (2008).
[8] Z. Ren, A. A. Taskin, S. Sasaki, K. Segawa, and Y. Ando, Phys. Rev. B **82**, 241306 (2010).
[9] J. L. Mi, M. Bremholm, M. Bianchi, K. Borup, S. Johnsen, M. Søndergaard, D. Guan, R. C. Hatch, P. Hofmann,and B. B. Iversen, Adv. Mater. **25**, 889 (2012).
[10] H. Kaibe, Y. Tanaka, M. Sakata, and I. Nishida, J. Phys. Chem. Solids **50**, 945 (1989).
[11] S. S. Kim, F. Yin, and Y. Kagawa, J. Alloy. Compd. **419**, 306 (2006).
[12] J. J. Shen, L. P. Hu, T. J. Zhu, and X. B. Zhao, Appl. Phys. Lett. **99**, 124102 (2011).
[13] C.-L. Chen, H. Wang, Y.-Y. Chen, T. Day, and G. J. Snyder, J. Mater. Chem. A **2**, 11171 (2014).
[14] L.-D. Zhao, S.-H. Lo, Y. Zhang, H. Sun, G. Tan, C. Uher, C. Wolverton, V. P. Dravid, and M. G. Kanatzidis, Nature (London) **508**, 373 (2014).
[15] H. Wang, W. Porter, H. Böttner, J. König, L. Chen, S. Bai, T. Tritt, A. Mayolet, J. Senawiratne, C. Smith, F. Harris, P. Gilbert, J. Sharp, J. Lo, H. Kleinke, and L. Kiss, J. Electron. Mater. **42**, 654 (2013).
[16] H. Wang, W. Porter, H. Böttner, J. König, L. Chen, S. Bai, T. Tritt, A. Mayolet, J. Senawiratne, C. Smith, F. Harris, P. Gilbert, J. Sharp, J. Lo, H. Kleinke, and L. Kiss, J. Electron. Mater. **42**, 1073 (2013).
[17] Y. C. Akgoz and G. A. Saunders, J. Phys. C **8**, 2962 (1975).
[18] Y. C. Akgoz and G. A. Saunders, J. Phys. C **8**, 1387 (1975).
[19] L. J. van der Pauw, Philips Res. Rep. **13**, 1 (1958).
[20] L. J. van der Pauw, Philips Tech. Rev. **20**, 220 (1958).
[21] K. A. Borup, E. S. Toberer, L. D. Zoltan, G. Nakatsukasa, M. Errico, J.-P. Fleurial, B. B. Iversen, and G. J. Snyder, Rev. Sci. Instrum. **83**, 123902 (2012).
[22] W. L. V. Price, Solid-State Electron. **16**, 753 (1973).
[23] O. Bierwagen, R. Pomraenke, S. Eilers, and W. T. Masselink, Phys. Rev. B **70**, 165307 (2004).
[24] J. Kleiza and V. Kleiza, Electron. Elect. Eng. **59**, 51 (2005).
[25] J. Kleiza and V. Kleiza, Lith. J. Phys. **45**, 333 (2005).
[26] J. Kleiza, M. Sapagovas, and V. Kleiza, Informatica **18**, 253 (2007).
[27] S. Ašmontas, V. Kleiza, and J. Kleiza, Acta Phys. Pol. A **113**, 1559 (2008).
[28] J. Kleiza and V. Kleiza, Acta Phys. Pol. A **119**, 148 (2011).
[29] L. J. van der Pauw, Philips Res. Rep. **16**, 187 (1961).
[30] See Supplemental Material at http://link.aps.org/supplemental/10.1103/PhysRevB.92.045210 for relevant derivations, discussion of numerical calculations, and possible error sources.
[31] R. Spal, J. Appl. Phys. **51**, 4221 (1980).
[32] H. H. Sample, W. J. Bruno, S. B. Sample, and E. K. Sichel, J. Appl. Phys. **61**, 1079 (1987).
[33] V. I. Fistul, *Heavily Doped Semiconductors* (Plenum Press, New York, 1969).
[34] J. Kleiza and V. Kleiza, Lith. Math. J. **38**, 232 (1998).
[35] C. Kasl and M. J. R. Hoch, Rev. Sci. Instrum. **76**, 033907 (2005).
[36] H. Holseth and A. Kjekshus, Acta Chem. Scand. **22**, 3284 (1968).